

# Data Augmentation, Multimodality, Subject and Activity Specificity Improve Wearable Electrocardiogram Denoising with Autoencoders

João Areias Saraiva<sup>1,2,3</sup> <sup>a</sup>, Mariana Abreu<sup>1,3</sup> <sup>b</sup>, Ana Sofia Carmo<sup>1,3</sup> <sup>c</sup>, Ana Fred<sup>1,3</sup> <sup>d</sup>  
and Hugo Plácido da Silva<sup>1,3</sup> <sup>e</sup>

<sup>1</sup>Department of Bioengineering, Instituto Superior Técnico, University of Lisbon, Portugal

<sup>2</sup>Department of Computer Science and Engineering, Instituto Superior Técnico, University of Lisbon, Portugal

<sup>3</sup>Pattern and Image Analysis Group, Instituto de Telecomunicações, Portugal

**Keywords:** Biosignal Denoising, Electrocardiogram, Accelerometry, Ambulatory Wearables, Data Augmentation.

**Abstract:** Event detection based on biosignals continuously acquired by wearable devices has become an emergent topic. Particularly, real-time event detection with the electrocardiogram (ECG) has been explored to monitor heart conditions and epileptic seizures in the ambulatory. However, ECG acquired in the ambulatory is much more prone to noise and artifacts, due to the dynamic nature of these environments. Therefore, real-time and robust ECG denoising methods are crucial if event detection is meant to succeed. Denoising autoencoders (DAEs) are studied as robust and fast methods to attenuate ECG noise and artifacts. ECG data augmentation techniques are shown to effectively improve the performance of such a deep learning method. Activity and subject specific models are shown to output better ECG denoised estimates, than non-specific ones. And using accelerometry (ACC) as noise reference exemplifies how biosignal multimodality improves ECG attenuation of muscle and motion artifacts. Therefore, this work establishes effective design techniques to be considered when engineering ECG deep learning models.

## 1 INTRODUCTION

Portable electrocardiography for the ambulatory is currently a necessity to monitor patients outside the hospital (Bansal and Joshi, 2018; Bayoumy et al., 2021). At the same time, automation of that monitoring has become an emerging topic (Prieto-Avalos et al., 2022), since human professional monitoring is infeasible at all times. Events of interest to be detected in real-time are, for instance, atrial fibrillation (Abu-Alrub et al., 2022), heart failure (Chen et al., 2021), epileptic seizures (Vandecasteele et al., 2021), and falls (Butt et al., 2021). Even for non-medical use, commercial wearable devices to continuously record the electrocardiogram (ECG), have been marketed for fitness purposes (e.g., *Fitbit*<sup>1</sup>), or even

for everyday check-ups (e.g., *Withings Move*<sup>2</sup>).

However, the ambulatory recording of ECG presents its challenges, primarily because the environment outside the hospital is dynamic and uncontrolled (Rodrigues et al., 2017). Therefore, and adding up to the fact that wearable hardware is usually less robust than clinical-grade instruments, the ECG acquired in the ambulatory is more likely to become contaminated with noise and artifacts (Chatterjee et al., 2020). A highly distorted ECG signal will interfere with the ability of any event detection algorithm to correctly interpret it, and, consequently, event detection will fail (Mohd Apani et al., 2020). If that would be the case, and if the clinical team is counting on the wearable to make informed decisions, those will become conditioned, and the patient's clinical condition can become compromised. Therefore, before event detection takes place, real-time robust ECG denoising constitutes an important preprocessing step.

Denoising autoencoders (DAEs) have been widely proposed to denoise the ECG (Arsene, 2020; Nurmainsi et al., 2020; Xiong et al., 2015; Chiang et al.,

<sup>a</sup>  <https://orcid.org/0000-0003-3715-0304>

<sup>b</sup>  <https://orcid.org/0000-0002-9340-6610>

<sup>c</sup>  <https://orcid.org/0000-0001-7954-3718>

<sup>d</sup>  <https://orcid.org/0000-0003-1320-5024>

<sup>e</sup>  <https://orcid.org/0000-0001-6764-8432>

<sup>1</sup> [fitbit.com](https://www.fitbit.com); accessed in Nov 2022

<sup>2</sup> [withings.com/withings-move](https://www.withings.com/withings-move); accessed in Nov 2022

2019; Reljin et al., 2020). These works have achieved great performances, however usually synthetic or real noise time series are retrospectively added to the clean ECG, which simplifies the DAE task to undoing an additive operation. In contrast, this work proposes a framework to train DAEs to map noisy ECG acquired with wearable electrodes to the simultaneously acquired ECG with gel electrodes.

We found out that, in this way, the denoising task becomes much more difficult, for the goal is no longer to merely undo a linear operation, but rather to attenuate non-stationary noise processes that may interact with each other in non-linear ways. Hence, additionally, design techniques were studied to improve DAE performance, namely data augmentation, activity and subject specificity, and multimodality. It is hypothesised that these are four crucial design techniques that should always be followed when engineering ECG deep learning models:

**Data Augmentation.** Deep learning (DL) models must be trained with a high number of labelled examples (Goodfellow et al., 2016). On the one hand, the number of examples needs to be large enough so that the model is able to generalise well. On the other hand, the train examples need to be representative of the heterogeneity the model will be tested against, otherwise it may lead to overfitting; but they also cannot be too heterogeneous, otherwise it may lead to underfitting. Overfitting and underfitting phenomena must be avoided when engineering machine learning (ML) models, and they can be prevented with a high number of examples balanced in heterogeneity. A common problem in training these models is, therefore, to access large datasets, correctly labelled, with balanced heterogeneity, particularly for biosignal datasets. A popular approach to solve this is to expand the datasets using data augmentation techniques (Pan et al., 2020; Huerta et al., 2021).

**Activity-Specific Models.** The ECG acquired while subjects execute different daily life activities is prone to contain very specific noise processes, resulting from the specific form of motion those activities introduce. It is hypothesised that these noise processes are somewhat similar for each activity. If so, DAEs should, in theory, be better at denoising ECG of a given activity if trained only with ECGs of that activity. These are called activity-specific models.

**Subject-Specific Models.** Subject variability is also responsible for different ECG waveforms and noise processes (Ashley and Niebauer, 2004), related with physiological and anatomical variance, or the individual way a subject executes an activity, or even the way they wear the device. Hence, subject-specific

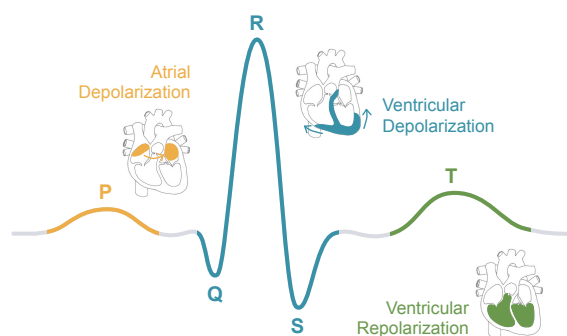


Figure 1: Illustration of a typical ECG waveform. QRS complex (in blue) refers to the Q, R and S curves together.

DAEs are hypothesised to perform better than subject-independent ones.

**Multimodality.** Employment of multiple biosignal modalities, such as respiration (An et al., 2022), and accelerometry (ACC) (Raya and Sison, 2002; Abecassis et al., 2018), has shown to be of added value; in a denoising task this is often coined a noise-reference. In this work, it is hypothesised that ACC contains useful motion information that can be used to attenuate motion artifacts present on the ECG.

The remainder of the article is organised as follows. Section 2 introduces the background on chest ECG, the common noise processes it presents, how its overall quality can be mathematically evaluated, and how chest ACC can serve as a complementary way to document the torso physiology. Section 3 describes how chest ECG and ACC were experimentally acquired with volunteers performing everyday tasks. Section 4 introduces the DAE architecture used to test these hypotheses and its general training process. Finally, the remaining sections discuss the impact of the techniques introduced before: data augmentation in Section 5.1, activity specificity in Section 5.2, subject specificity in Section 5.3, and multimodality in the training process in Section 5.4. Conclusions and applications are discussed in Section 6.

## 2 WEARABLE ELECTROCARDIOGRAMS

The ECG measures the electrical activity of the heart at the body surface. The recorded biosignal corresponds to changes in the polarisation of cardiac muscle tissue, which is responsible for the coordinated contraction of the heart. Cardiomyocytes are depolarised by the action potentials generated by a specialised conducting system, giving rise to the different phases of the cardiac cycle. Each cardiac cycle is comprised of three stages: the atrial contraction, the

inter-ventricular propagation, and the ventricular contraction (Ashley and Niebauer, 2004). In the absence of cardiac dysfunctions, the electrocardiogram (ECG) signal presents a characteristic pattern, depicted in Figure 1, which comprises five main waves – P, Q, R, S and T – that are produced by those three stages.

A clinical-grade ECG would be acquired by attaching two to ten wet electrodes on the chest and limbs, each providing a different view angle and direction – a lead – from which it acquires the heart depolarisation. However, ambulatory and wearable devices usually do not acquire signals with twelve leads, but rather with just one or two on the chest, abdomen or left upper limbs. Also, wearables often use dry electrodes, whereas in clinical units wet electrodes are used (Bansal and Joshi, 2018).

From the ECG time series, it is usually derived another one called the R-R peak interval (RRI) time series. This corresponds to the time difference between each consecutive pair of R peaks. From the RRI, the heart rate variability (HRV) features are commonly extracted, which is a set of statistics, rich in physiological information, that can serve as biomarkers for the detection of events of interest (Behbahani et al., 2013). Since the computation of the RRI relies on the accurate identification of the R peaks, it is crucial for event detection algorithms that ECG segments present enough quality for the identification of all R peaks. Even for highly contaminated ECG segments, they can still be of value for event detection if the R peaks are identifiable (Munoz-Minjares et al., 2021).

## 2.1 Noise and Artifacts Present in ECG

Electrodes capture any electrical potentials, whatever they are, and do not distinguish between what truly is our signal of interest and everything else that is not. So, when acquiring ECG, specially with dry electrodes, the ECG trace is susceptible to numerous noise and artifact sources. Background noise,  $\eta$ , and the signal of interest,  $y$ , are usually additive, which means that both components superimpose each other and may become indistinguishable in the acquired time series,  $x$ , that is,  $x[n] = y[n] + \eta[n]$ . Next are introduced the common noise processes described in the literature (Semmlow and Griffel, 2014).

**Power-line Interference (PLI).** Offsets due to electrical couplings between external electromagnetic fields and the human body (50Hz in Europe and 60Hz in the US). The most traditional and simple method to remove PLI is to apply a notch filter (Kutz, 2010).

**Baseline Wander (BW).** Pressure on the electrodes during acquisition will cause deformation of the

skin and, consequently, variations in skin impedance, which, in turn, will create an offset potential in the acquired signal. Also, chest and diaphragm movement due to respiration, gastrointestinal movements, and normal gaiting are sufficient to induce BW. Respiration movements of the rib cage produce a *wander* on the base axis of the recorded ECG trace, that is, the baseline *moves* up and down, rather than maintaining constant. This can cause T waves to be higher than R waves, which may end up being detected as false R peaks (Kutz, 2010). The BW spectrum is usually lower than 0.5–1 Hz, hence the most traditional way to remove it being with a highpass filter. However, if it presents spiky or trendy structures, losing its quasi-sinusoidal morphology, a highpass filter can come as a naive strategy (Mohaddes et al., 2020).

**Myogenic Noise (EMG).** Generated by skeletal muscle activity. EMG typically ranges from 10 Hz to 5 kHz, whereas the ECG typically ranges from 0.05 Hz to 100 Hz (Kutz, 2010). Hence, at least up to a point, both biosignals can be separated in the frequency domain. Traditionally, bandpass filters are used to attenuate EMG noise; however EMG is a nonstationary and nonlinear biopotential (Mohaddes et al., 2020), so this is often an insufficient effort.

**Electrodermal Noise (EDA).** Accumulation of sweat under the electrodes changes the skin impedance, in turn changing the skin electrical potential. This noisy offset varies in a pressure, temperature, hydration, and time dependent manner, hence the superimposed drifts can be difficult to remove from low-frequency ECG components (Kutz, 2010).

**Motion Artifacts (MAs).** In daily life activities, limbs and trunk movement and normal gaiting can create artifacts in the ECG that look like physiological features, although they are not. This kind of movements can be seen as a nonstationary and nonlinear process (Mohaddes et al., 2020). Dry electrodes are particularly prone to MAs, because upon motion electrodes often stop touching the skin for a few moments, creating an air gap, which translates into an increased capacitance in the interface. Conversely, the gel present in wet electrodes helps to minimise impedance variations caused by MAs (Kutz, 2010).

## 2.2 ECG Signal Quality Indexes

Two ECG signal quality indexes (SQIs) (Clifford et al., 2012; Li et al., 2007; Li et al., 2014) can be used to empirically evaluate the ECG quality. The first is the kurtosis signal quality index (kSQI):

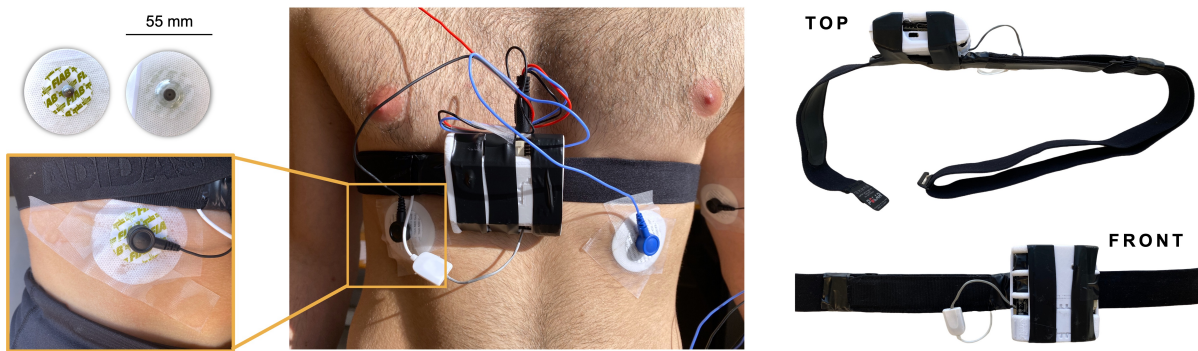


Figure 2: Biosignal acquisition setup. Left: chest electrocardiogram acquired with dry electrodes embedded in the band textile (Band-ECG) and chest electrocardiogram acquired with gel electrodes (Gel-ECG) placement. Right: Body location of all modalities.

$$kSQI = \frac{E\{(y - \bar{y})^4\}}{\sigma_y^4}, \quad (1)$$

where  $\mathbf{y}$  is any ECG signal,  $\bar{y}$  its mean,  $\sigma_y$  its standard deviation, and  $E\{\cdot\}$  is the expected value, i.e., the average. It evaluates the absence of noise in general, and segments with  $kSQI \leq 5$  present high levels of noise and unsatisfactory quality. The second SQI is the R-quantity signal quality index (qSQI), which quantifies the agreement of any two R-peak detection algorithms with the ratio:

$$qSQI = \frac{2R}{R_1 + R_2}, \quad (2)$$

where  $R_1$  and  $R_2$  are the number of R peaks detected by each of the chosen algorithms, and  $R$  is the number of R peaks detected in common by both algorithms, assumed to be the true number of R peaks. ECG segments with  $qSQI > 0.9$  can be considered with satisfactory quality. In this work, the R-peaks detectors used to compute qSQI were the Hamilton algorithm (Hamilton, 2002) and the Christov algorithm (Christov, 2004), as suggested in (Saraiva, 2022a).

### 2.3 Chest and Torso Movement

Chest ACC can be acquired to complement the ECG. ACC sensors convert motion into electrical voltage based on the gauge effect, capacitive, or piezoelectric physical phenomena. The recorded signals are usually measured in meters per squared second ( $m.s^{-2}$ ) or g-force units ( $1g \approx 9.81m.s^{-2}$ ) (Kavanagh and Menz, 2008). Usually, three ACC channels are acquired, one per each dimension of the physical space, which allow us to extract translational and rotational information about the torso movement.

## 3 EXPERIMENTAL DATASET ACQUISITION

An acquisition protocol was devised to collect human biosignals in dynamic environments, which was approved by the Ethics Committee of Instituto Superior Técnico, with the reference 22/2022. A set of 17 subjects volunteered to participate in our biosignal acquisition sessions. The cohort comprehends 59% male and 41% female Caucasian subjects. The median age is 24 years old, with the younger subject having 18 and the older subject having 57 years old. At the time of acquisition, eleven subjects had recovered from a COVID-19 infection in the previous six months. No subject had a history of cardiac disease, implanted devices, pain or difficulty in breathing. Every subject participated voluntarily in this study, having signed an informed consent, that authorises the use and sharing of all data for research.

### 3.1 Hardware Setup

A chestband device was crafted out of a ScientISST board<sup>3</sup> for the purpose of this study. ScientISST boards are general-purpose biosignal acquisition boards, which can be modified according to research needs. Four sensors were soldered to four analogue channels of the board: two ECG sensors, a 3-axis ACC sensor, and a respiration sensor. All sensors acquired the respective biosignals at a sampling frequency of 300 Hz.

The ScientISST board, the sensors and all associated hardware were embodied into a textile chestband from Polar<sup>4</sup>, similar to the ones our group uses to monitor patients with epilepsy at the hospital (Carmo

<sup>3</sup>scientisst.com/sense; accessed in Dec 2022

<sup>4</sup>polar.com/en/products/accessories/polar-soft-strap; accessed in Dec 2022



Figure 3: Proposed ECG denoising pipeline. Inputs: Noisy ECG and correspondent ACC. Output: Denoised ECG estimate.

Table 1: Useful recorded duration (in minutes) in each session.

A	B	C	D	E	F	G	H	I	J	K	L	M	N	O	P	Q	R
45.2	27.6	46.1	39.9	31.7	36.1	41.1	31.05	36.1	40.4	41.1	44.4	16.4	17.6	45.4	15.0	47.8	33.1

et al., 2022). One ECG sensor was connected to the dry conductive plastic electrodes of the chestband, hence from herein it will be referred to as Band-ECG. The other ECG sensor was connected to disposable wet electrodes, hence it will be referred to as Gel-ECG. Two of the wet electrodes were placed contralaterally on the chest (Lead I), mirroring the textile electrodes. The ground electrode was placed on the left iliac crest. Since the activities performed in these acquisitions involved high-amplitude movement and high sweat release, the Gel-ECG wet electrodes were secured in place with Transpore surgical tape, contrarily to the wearable dry electrodes. As will become clear ahead, the Gel-ECG signal will be used as ground-truth of the Band-ECG signal. Hence, both were placed to capture identical Lead I ECG, as depicted in Figure 2.

### 3.2 Preprocessing

Both ECG sensors included an analogue [0.5, 40] Hz passband filter. Two median filters were applied to the Band-ECG time series, to estimate BW, the output of which was subtracted from the original ECG, resulting in BW-free time series. This preprocessing has been validated in previous works (Xia et al., 2018; Saraiva, 2022b), for robust real-time BW denoising of ECG acquired in nonstationary and uncontrolled environments. Hence, the following experiments on the Band-ECG start from with this preprocessed time series, as illustrated in Figure 3.

The Gel-ECG time series were enhanced with a FIR filter of [1.2, 40] Hz passing band and order of 250. This is because the Gel-ECG channel will serve as ground-truth of Lead I ECG of each subject.

No filtering was applied to the ACC time series, as conveyed in Figure 3.

### 3.3 Acquisition Protocol

In each session, the volunteers were asked to orderly perform the following activities:

1. **Lift:** To repeatedly lift a heavy object;
2. **Greetings:** To repeatedly handshake and to wave;
3. **Gesticulate:** To gesticulate while talking;
4. **Jumps:** To jump repeatedly;
5. **Walk-Before:** To walk outside before running;
6. **Run:** To run outside;
7. **Walk-After:** To walk outside after running.

This protocol was considered to be illustrative of daily life activities that are prone to hinder ECG quality. These activities either due to excessive sweat release, associated motion, or both, usually lead to noise and artifacts in the recorded biosignals.

For different reasons, not all subjects performed all activities, and the running and walking durations were different for each subject. Table 1 shows the useful recorded duration of each session. One of the subjects volunteered for two sessions on different days, hence there are a total of 18 sessions, identified from A to R. In each session, a median of 55 useful minutes were recorded, summing up to a cohort total of 10.58 hours. By "useful" it should be understood "after discarding the periods in which no activity was being executed".

### 3.4 Initial Quality Assessment

Cohort median kSQI of Band-ECG channels was 3.5 times lower than that of Gel-ECG signals, conveying that more noise was present on the wearable-like ECG. Particularly, *Lift*, *Jumps*, *Run*, and *Walk-After* segments showed unacceptable kSQI below 5. Moreover, the median R peak detection agreement of two detectors (qSQI) was 1.00 when using Gel-ECG for all activities, except *Jumps* (0.98), whereas using Band-ECG signals was 0.96 on average. In particular, *Run* segments showed qSQI below 0.9 for Band-ECG signals. Therefore, the ECG acquired with the chest band presents as noisier and with poorer quality than that acquired with gel electrodes, not necessarily just because of the differences in hardware, but also due to its resilience to the executed activities.

## 4 DENOISING AUTOENCODER

DAEs were designed to attenuate EMG noise, EDA noise, MAs, and any other type of process that deviates the Band-ECG waveform from that of the Gel-ECG. Unlike other denoising methods, DAEs alleviate the need to characterise the noise processes, and instead they estimate how a version of the signal without noise would look like (Goodfellow et al., 2016). This is because these models undergo a training process with the goal of learning an implicit representation of the ECG trace without noise. This representation is an internal state of neural network’s weights and biases (the model’s parameters) that, when applied to a noisy ECG segment, output a denoised version of it. These parameters are *learned* from large datasets of input (noisy) and output (clean) pairs.

### 4.1 Architecture

As aforementioned in Section 1, it is hypothesised that the motion information of the torso, present in the ACC time series, is correlated, causally or not, with the MAs present in the ECG time series, and that this information can be used to attenuate them. Hence, the DAE inputs are (4, 300) matrices, where 4 is the number of segments (1 ECG + 3 ACC), and 300 is the number of samples of each, which corresponds to 1 second. The ECG segment is timely synchronised with the ACC segment. Figure 4 illustrates these matrices, as well as the complete network architecture, which was inspired in (Abecassis et al., 2018). The network architecture is divided in two modules: encoder and decoder.

The encoder task is to represent the input segments in a latent space, that isolates noise and artifacts from the ECG process. In our approach, the encoder module has four layers. The input passes first by a 2D convolutional layer that extracts 8 features with a kernel of size (4, 7). In this process, the kernel strides (or *shifts*) every 1 sample. Additionally, three samples of padding are added to each input. The activation function of this layer is the hyperbolic tangent. Then, a maximum pooling layer of kernel size (2, 1), which strides by two, selects the maximum of each pair of values in each feature, reducing the feature length from 300 to 150. A second 2D convolutional layer extracts 4 features using a kernel size (3, 1), which strides by one. One value of padding is added to each input feature. The same activation function is used of this layer. A second maximum pooling layer, equivalent to the one before, selects the maximum of each pair of values in each feature, reducing the feature length from 150 to 75. Therefore, the la-



Figure 4: Proposed DAE architecture. Kernel sizes on the right side of each layer. Tensor sizes in (C, H, W) format.

tent space has a size of 4 features of 75 points each, i.e., downsampling occurs from 300 to 75 points.

The decoder task is to recover the segment to the original space, potentially outputting a denoised version of the input. The decoder module has three 2D transpose convolutional layers, that reverse the encoder process. The first layer takes 4 features and outputs 8, using a kernel of size (3, 1). It strides by two and outputs with (1, 0) padding, increasing the feature length from 75 to 150. The second layer also outputs 8 features, using a kernel of size (3, 1). It strides by two and outputs with (1, 0) padding, increasing the feature length from 150 to 300. These two layers are activated by the hyperbolic tangent. The last layer encompasses the 8 features into 1, using a kernel of size (3, 1), and has no activation function. Its output is the potentially denoised ECG segment.

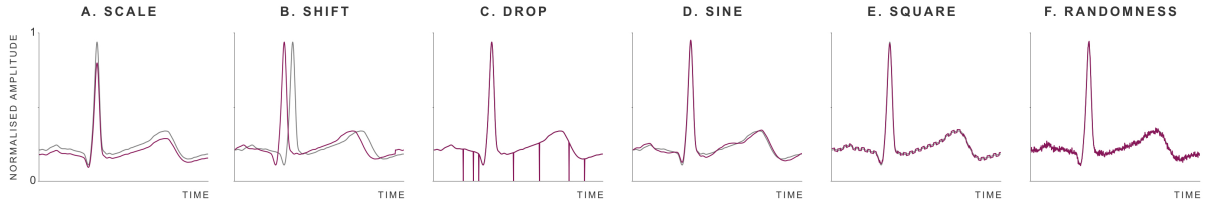


Figure 5: Examples of derived ECG segments when applying data augmentation techniques, in pink. Original time series in grey. Scale  $M = 0.85$ . Shift  $D = 0.05$ . Drop  $p = 0.02$ . Sine  $A = 0.02$ . Square  $A = 0.01$ . Randomness  $A = 0.01$ . Illustrative heartbeat segment of 700 ms.

## 4.2 Training and Evaluation

The DAEs were trained using the Adam optimizer (Kingma and Ba, 2014). Each network was allowed to be trained for as many epochs as needed until convergence was reached. Convergence was defined by the validation loss not decreasing for 20 epochs. The output loss of each iteration was computed using the mean squared error (MSE) against the targets, which were the corresponding Gel-ECG segments. Essentially, given an *object* (Band-ECG, ACC) the network should output a segment with minimal error against the pair *target* (Gel-ECG). In each experiment, the examples (*object*, *target*) were divided in 20%, trimmed from the centre of each time series, for the test dataset, and the remaining 80% of segments would constitute the train dataset. The train:validation ratio was 8:2.

The denoised estimates,  $\hat{\mathbf{y}}$ , were compared with their timely corresponding Gel-ECG segment,  $\mathbf{y}$ , using the normalized mean squared error (NMSE):

$$NMSE (dB) := 10 \cdot \log_{10} \frac{\|\mathbf{y} - \hat{\mathbf{y}}\|_2^2}{\|\mathbf{y} - \bar{\mathbf{y}}\|_2^2}. \quad (3)$$

This metric is similar to the MSE, in the sense that the estimation squared errors are in the numerator, and the normalisation factor in the denominator. The normalisation factor is the squared errors of the signal's mean constant function. Hence, semantically, the NMSE tells us *how good* the denoised estimate is in comparison with the signal's mean. If the NMSE is negative, the denoised estimate error is smaller than the signal's mean error – which is the desirable. Contrarily, if the NMSE is positive, then the signal's mean predicts the true signal better than the denoised estimate – which is the undesirable.

Additionally, the ECG SQIs previously described in Section 2.2 were used to compare the quality of Band-ECG segments before and after denoising.

## 5 RESULTS AND DISCUSSION

This section addresses the research questions raised in Section 1, in the same order they were introduced. The ECG process can be thought of comprehending three main sources of variability:

- **Environmental:** Electrode variability, pressure, hydration, temperature, and skin conductance introduce variability to the ECG trace. This is addressed, not only, but primarily, in Subsection 5.1.
- **Activity:** If the subject is at rest or performing an activity of some pattern, it introduces variability to the ECG. This is explored in Subsection 5.2.
- **Subject:** The subject's physiology and own way of wearing the chestband introduce variability to the ECG trace. This is explored in Subsection 5.3.

### 5.1 Impact of Data Augmentation

The techniques recently suggested in (Nonaka and Seita, 2022) were implemented to augment the number of ECG and ACC segments of each activity. Given a biosignal segment, similar segments were derived, without significantly altering its original natural morphology, by applying the following operations:

- **Scale:** Contraction or dillation, in amplitude, by a multiplier,  $M$  (Figure 5A).
- **Shift:** Left or right translation, in time, by  $D \times$  number of samples (Figure 5B).
- **Drop:** Multiplication of each sample by zero with probability  $p$  (Figure 5C).
- **Sine:** Addition of a sinusoidal wave of random frequency,  $f$ , and amplitude  $A$  (Figure 5D).
- **Square:** Addition of a square pulse of random frequency,  $f$ , and amplitude  $A$  (Figure 5E).
- **Randomness:** Addition of gaussian noise of amplitude  $A$  (Figure 5F).

Parameter  $M$ , in Scale, should be between  $[0.25, 1[$  for contraction or between  $]1, 4]$  for dilation. Parameter  $D$ , in Shift, should be between  $]0, 1[$ . The maximum displacement is achieved when  $D = 0.5$ . The

Table 2: Average test losses of DAEs trained with datasets augmented "Multiplier" times, grouped by augmentation technique. Values in  $\times 10^{-3}$ .

Multiplier	Scale	Shift	Drop	Sine	Square	Randomness	All
10	178.23	111.43	140.82	91.943	81.306	82.924	42.534
50	101.40	93.354	84.532	62.463	41.050	43.263	26.135
100	57.343	49.935	61.930	34.928	22.856	27.050	14.938

shift direction (left or right) is random. Parameter  $p$ , in Drop, should be between  $]0, 1[$ , since it is a probability. Parameter  $A$  should be between  $]0, 1[$  in Sine,  $]0, 0.02[$  in Square and Randomness, so that the natural biosignal morphology does not get significantly altered. Frequency  $f$  is random between  $[0.001, 0.02]$  in Sine, and between  $[0.001, 0.1]$  in Square. As illustrated in Figure 5, the derived segments (in pink) could have very well been acquired in a real scenario, due to environmental variability.

**Universal DAE.** On a first basis, a DAE to be used for all subjects and for all activities was trained only with real examples. There are 37821 examples in the dataset, which correspond to the total number of seconds reported in Table 1. Herein this and the other models presented in this subsection will be termed universal DAEs. The model was trained for 262 epochs, in batches of 64 examples, and initial learning rate of 0.0005. An average test loss of 0.5305 was achieved, which is not satisfactory, since the biosignals were normalised in amplitude between 0 and 1.

**Different Augmentation Multipliers.** The dataset of real examples was then linearly augmented 10 times with each of the six described techniques, resulting in six augmented datasets, each containing 416031 examples, which corresponds to eleven times the number of real examples. Six DAEs were trained and tested with each of these augmented datasets, in the same conditions as before, and the average test losses are reported in Table 2. The test loss decreased when using each of these augmented datasets. The same experiment was repeated with datasets augmented 50 times with the same techniques, and test losses further decreased for every model. Repeating the experiment with datasets augmented 100 times also further reduced the test losses of every model, to one order of magnitude lower than that of the universal DAE.

**Different Augmentation Techniques.** Neural networks by nature lack explainability, however, in an attempt to understand these results, one might attribute the success of *Sine*, *Square*, and *Randomness* techniques (Table 2) to the fact that they actually generate different examples in a nonlinear way, that cannot be traced back to the original examples,

unless the augmentative process that was added is kept stored, therefore increasing environmental variability in a nonlinear way. Conversely, *Scale*, *Shift*, and *Drop* techniques apply linear transformations or nullify some samples. *Scale* contracts or expands the biosignals' amplitude, which occurs in real environments, but most of the waveform characteristics are still the same. *Shift* translates segments in time, which could be achieved by nothing more than segmenting the biosignals in a different way. For this reason, from the next subsection forward only *Sine*, *Square*, and *Randomness* techniques are employed. It might seem paradoxical to increase environmental variability, however the dramatic increase in the number of examples allows the models to implicitly capture these environmental differences and to discriminate them from the ECG pattern, consequently leading to better generalisations and to avoid underfitting.

**All Augmentation Techniques.** Another experiment was conducted by augmenting the original dataset all-together with the six techniques, 10, 50 and 100 times. These datasets contained approximately more than 2.6, 13.2, 26.5 million examples, respectively. The test losses can be found in the last column of Table 2. It can be concluded that the test loss decreases by increasing the dataset size. However, for the dataset augmented 100 times, the test loss (0.0149) is only 0.0079 lower than the best result achieved with a dataset generated by a unique technique (*Square*, 0.0229), hinting that more examples do not necessarily lead to significant improvements. Comparisons aside, a test loss of 0.0149 may still not be satisfactory, as shall be discussed later. In this case, since segments are normalised in amplitude between 0 and 1, such a loss represents a 1.5% deviation from the targets, which in artifacts can still appear to be quite noisy. Activity and subject specificity strategies are explored ahead to improve the denoising performance. Meanwhile, the impact of data augmentation will continue to be addressed.

## 5.2 Impact of Activity Specificity

The full dataset was divided by activity, including *Baseline* when the subjects were at rest in the beginning of the session, into smaller datasets, that is, eight

datasets with the number of examples indicated in Table 3. Each of these activity-specific datasets was also augmented 50 and 100 times, using *Sine*, *Square*, and *Randomness*. For each of these, a DAE was trained for at most 150 epochs, in the same conditions as before. The test losses are given in Table 4.

Table 3: Total useful duration, in seconds, of each activity.

<i>Lift</i>	<i>Greetings</i>	<i>Gesticulate</i>	<i>Jumps</i>	<i>Walk-B</i>	<i>Run</i>	<i>Walk-A</i>
1262	767	1469	132	2970	26953	2697

When no data augmentation is applied, and only real examples are used to train the activity-specific DAEs, the average test losses are two orders of magnitude lower than that of the best universal DAE. When the datasets of each activity are augmented, the average test losses are one order of magnitude lower than the universal DAEs trained with an augmented dataset. Concretely, the average test loss is 2.5 times smaller for *Run* DAEs and 12 times smaller for *Baseline* DAEs. *Gesticulate* and *Greetings* models achieved the lower test losses. Therefore, activity-specific DAEs perform better than non-specific ones, at least up to the point of subject variability in task execution and the environmental differences.

### 5.3 Impact of Subject Specificity

Assuming each subject’s dataset is representative enough to capture the different ways they can execute an activity, the full dataset was divided by subject and by activity into smaller datasets, so that only environmental conditions could influence the denoising process. Hence,  $A$  datasets per subject, being  $A$  the number of activities recorded with each subject. Each of these datasets was augmented 100 times, using *Sine*, *Square*, and *Randomness* techniques. For each of these, a DAE was trained in the same conditions as before. The test losses are reported in the first row of Table 5.

Inspecting the cohort median, when training is specific of the subject, the average test loss is one order of magnitude lower for all activities, except for *Jumps* and *Run*, than that of the subject-independent activity-specific models. *Jumps* and *Run* segments continue to be the most challenging to denoise, similarly to Table 4. Nonetheless, for *Run* segments, a median 0.119% deviation from the target is more acceptable than that achieved with a subject-independent DAE. And for some subjects, the *Run* test loss was one order of magnitude lower than that of subject-independent models, such as in session B (0.000429) and session O (0.000304) (not shown). Moreover,

*Baseline*’s loss also decreased one order of magnitude, and, similar to Table 4, it is the lowest test loss, which is expected since subjects were at rest in these periods. Therefore, subject-specific DAEs perform better than non-specific ones, at least up to the point of environmental differences.

### 5.4 Importance of Motion Information

One might question if the ACC segments, given along with the noisy ECG, actually contribute to the denoising process, or if the optimiser is minimising the loss between the noisy and target ECGs by training the networks to ignore the ACC inputs. The trained weights immediately after the input layer were checked and no evidence was found that, up to this level, the ACC inputs were being nullified. However, a much more fine inspection would have to take place in the remaining trained parameters to answer if and how this would occur. But we do not need to know how the networks use the ACC inputs in the denoising process, we simply need to know if they do. To overcome such a cumbersome study, the same activity and subject specific DAEs were retrained with no ACC information.

In this experiment, per each *object*, three time series were still fed to the network along with the noisy ECG – otherwise the architecture would have to change – but these time series were fabricated and were not the real ACC ones. To synthesise ACC, time series of the same length were generated with Gaussian noise of zero mean and unit standard deviation,  $\mathcal{N}(0,1)$ . The same example pairs of *objects* and *targets* were used, however the ACC segments of each *object* were replaced by the Gaussian time series, which has no real motion information. The dataset was augmented in the same way, and the models were trained under the same conditions. The median test losses can be found in the last row of Table 5. The test MSE in every activity is similar and in the same order of magnitude as the universal DAE, except for *Baseline* segments, meaning these models do not output satisfactory denoised estimates if the ACC-dedicated segments are not actually the chest ACC time series. It is understandable that *Baseline* models show lower MSE due to the absence of motion in the input segments during this period. Therefore, the ACC time series contain motion information regarding the chest that is useful to denoise ECG.

### 5.5 Final Design

The performance of the designed activity and subject specific models were validated in a real scenario,

Table 4: Average test losses of DAEs trained with activity-specific datasets, grouped by augmentation multiplier. Values in  $\times 10^{-3}$ .

Multiplier	Baseline	Lift	Greetings	Gesticulate	Jumps	Walk-Before	Run	Walk-After
0	1.660	2.903	4.153	1.723	3.394 <sup>1</sup>	3.395	6.381	3.743
50	1.343	2.530	2.034	1.430	3.249	2.991	6.283	2.901
100	1.005	2.000	1.487	1.037	3.027	2.543	5.918	2.396

<sup>1</sup> Trained in batches of 16 examples, because there were not enough examples.

Table 5: Cohort median of average test loss of DAEs trained with activity-specific and subject-specific datasets, grouped by activity. Former row: With real and augmented ACC; Later row: With no real ACC. Values in  $\times 10^{-3}$ .

	Baseline	Lift	Greetings	Gesticulate	Jumps	Walk-Before	Run	Walk-After
With ACC	0.172	0.442	0.286	0.211	1.264	0.553	1.198	0.706
No ACC	28.134	908.421	631.102	120.807	937.195	720.910	944.261	852.044

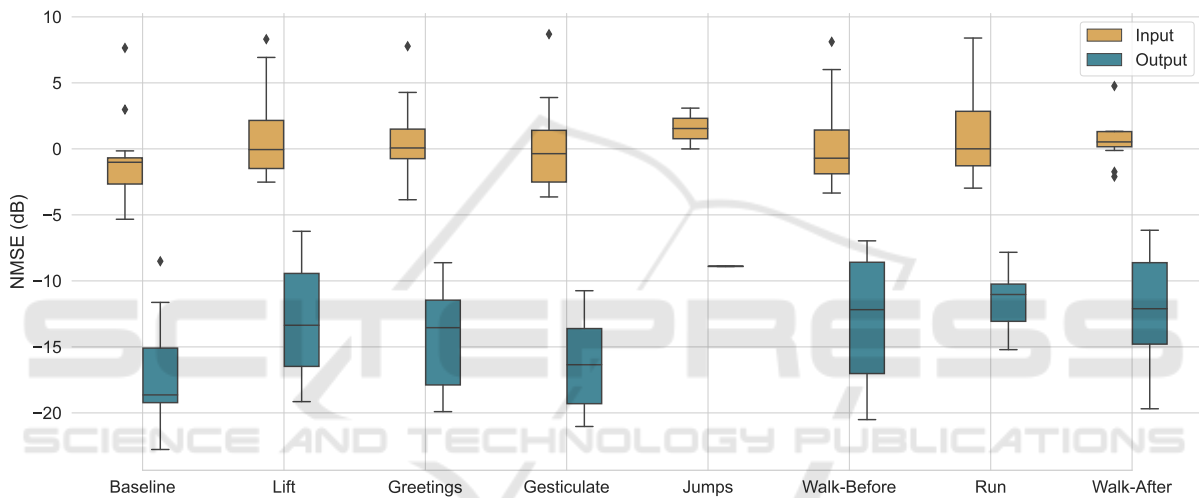


Figure 6: Improvement in NMSE of subject and activity specific DAEs tested only with real examples.

Table 6: Comparing ECG signal quality indexes (SQIs) before and after denoising steps, grouped by activity. Cohort Quartile 1 (Q1) and Quartile (Q3) values, in the format "Q1–Q3". Values in red are below satisfactory the specific SQI threshold.

	Baseline	Lift	Greetings	Gesticulate	Jumps	Walk-B	Run	Walk-A
kSQI Input	9.1–14.2	1.4–5.1	3.7–7.5	3.7–12.4	3.4–4.2	1.5–8.1	0.8–2.9	0.9–2.4
kSQI Output	12.4–22.1	10.0–16.5	12.4–20.1	10.1–19.5	11.1–11.3	10.9–15.8	11.3–14.5	9.2–17.3
qSQI Input	0.98–1.00	0.91–0.96	0.95–1.00	0.96–1.00	0.78–0.92	0.94–1.00	0.86–0.99	0.94–1.00
qSQI Output	1.00–1.00	0.94–1.00	0.97–1.00	1.00–1.00	0.97–0.98	0.97–1.00	0.95–1.00	0.98–1.00

where the networks are not tested with augmented examples. With the same trained parameters, each DAE was tested with the respective non-augmented test set, i.e., only with the real examples segmented from the original time series. For instance, the *Run* DAE of session F was tested with a time series of 4.28 minutes, whereas the *Lift* DAE was tested with only 29 seconds (cohort durations not shown). The NMSEs of these inputs and output denoised estimates against the Gel-ECG are compared in Figure 6. The

denoised median NMSE decreased below  $-10$  dB for all activities, and *Gesticulate* NMSE decreased below  $-15$  dB. *Gesticulate*, *Greetings* and *Lift* segments obtained the higher improvements, respectively,  $-15.9$ ,  $-13.6$  and  $-13.3$  dB. *Run* and *Jumps* segments obtained the lower improvements, although still valuable, of respectively,  $-11.0$  and  $-10.4$  dB. This indicates that the denoised estimations approximate better the Gel-ECG than the signal’s mean.

The first block of Table 6 shows that segments



Figure 7: Example of *Walk-Before* DAE of session Q. Potentially false R peaks highlighted in yellow.

from all activities, except *Baseline*, showed unacceptable kSQI before denoising (in red). After DAE denoising all interquartile kSQI increased. The median kSQI was higher than 11 for all activities after denoising, demonstrating there was less noise present in the Band-ECG segments after denoising. The second block of Table 6 shows that the R peaks agreement by two algorithms was below 0.9 in some *Jumps* and *Run* input segments (in red). After subject and activity denoising, the R peaks of these segments were more salient and unequivocally identified by the two different algorithms. Nearly all *Baseline* and *Gesticulate* segments showed 1.00 agreement. Therefore, removal of BW is not sufficient to make better R peak detections, and the DAE denoising process most contributed to accurate detections. As aforementioned, particularly in highly noisy environments, it is very important that R peaks can still be accurately detected in order to extract HRV features. Figure 7 shows an example of how multiple high-amplitude peaks were attenuated in walking activities. Such high-amplitude peaks could very well be mistakenly identified as R peaks. Moreover, in this example, Q and S waves were well pronounced in all heartbeats; and P and T waves were well corrected in most heartbeats, both in amplitude and in time, to approximate those of the Gel-ECG (*target*).

## 6 CONCLUSIONS

The training process of an ECG-based DAE architecture was studied. The best results for the test dataset were achieved when DAEs were trained specifically for each subject and each activity, with augmented datasets, and using chest ACC as noise-reference. Therefore, subject and activity specificity, data augmentation, and multimodality, together prove as effective design techniques to take into consideration when engineering ECG deep learning models.

It should be noted that it is data augmentation that possibilities the design of these specific models,

otherwise there would not be enough subject-specific and activity-specific examples for each subject, gathered from only 55 minutes (median) of multi-activity sessions. Hence, data augmentation enables subject-specific models even from short duration acquisitions.

Moreover, the proposed denoising method has two main advantages. Firstly, the ECG can be blindly segmented in real-time in 1-second segments, producing outputs with no ringing effects, therefore dispensing the need for R peak computation to segment the ECG by heartbeats. Secondly, the proposed DAE outputs denoised estimates in polynomial time, since the 2D convolution operation is majored at  $O(N^4)$ , where  $N$  is the segment number of samples, hence it is feasible for online denoising in wearables.

## ACKNOWLEDGEMENTS

This work was partially funded by the IST research grant BL88/2022, under the scope of project 1018P.06071.1.01.01 "CardioLeather", by the IT research grant BI16/2021, under the project PCIF/SSO/0163/2019 "SafeFire", and by the Fundação para a Ciência e Tecnologia (FCT) / Ministério da Ciência, Tecnologia e Ensino Superior (MCTES) research grants 2021.08297.BD and 2022.12369.BD, through national funds and when applicable co-funded by EU funds.

## REFERENCES

- Abecassis, L., Ho, M., Tit-Lartey, O., Hwang, W., Gathmann, T., Lum, Z., Loong, N. Y., and Moo, J. (2018). Machine Learning based Denoising of Electrocardiogram Signals from a Wearable ECG Monitor. BSc. Report, Imperial College London, Department of Bioengineering.
- Abu-Alrub, S., Strik, M., Ramirez, F. D., Moussaoui, N., Racine, H. P., Marchand, H., Buliard, S., Haïssaguerre, M., Ploux, S., and Bordachar, P. (2022). Smartwatch Electrocardiograms for Automated and Manual Diagnosis of Atrial Fibrillation: A Comparative Analysis of Three Models. *Front Cardiovasc Med*, 9:836375.
- An, X., Liu, Y., Zhao, Y., Lu, S., Stylios, G. K., and Liu, Q. (2022). Adaptive Motion Artifact Reduction in Wearable ECG Measurements Using Impedance Pneumography Signal. *Sensors*, 22(15):5493.
- Arsene, C. (2020). Design of Deep Convolutional Neural Network Architectures for Denoising Electrocardiographic Signals. In *2020 IEEE Conference on Computational Intelligence in Bioinformatics and Computational Biology (CIBCB)*, pages 1–8.

- Ashley, E. A. and Niebauer, J. (2004). *Conquering the ECG*. Remedica.
- Bansal, A. and Joshi, R. (2018). Portable out-of-hospital electrocardiography: A review of current technologies. *Journal of Arrhythmia*, 34(2):129–138.
- Bayoumy, K., Gaber, M., Elshafeey, A., Mhaimeed, O., Dineen, E. H., Marvel, F. A., Martin, S. S., Muse, E. D., Turakhia, M. P., Tarakji, K. G., and Elshazly, M. B. (2021). Smart wearable devices in cardiovascular care: Where we are and how to move forward. *Nat Rev Cardiol*, 18(8):581–599.
- Behbahani, S., Dabanloo, N. J., Nasrabadi, A. M., Teixeira, C. A., and Dourado, A. (2013). Pre-ictal heart rate variability assessment of epileptic seizures by means of linear and non-linear analyses. *Anatolian Journal of Cardiology*, 13(8):797–803.
- Butt, F. S., La Blunda, L., Wagner, M. F., Schäfer, J., Medina-Bulo, I., and Gómez-Ullate, D. (2021). Fall Detection from Electrocardiogram (ECG) Signals and Classification by Deep Transfer Learning. *Information*, 12(2):63.
- Carmo, A. S., Abreu, M., Fred, A. L. N., and da Silva, H. P. (2022). EpiBOX: An Automated Platform for Long-Term Biosignal Collection. *Front. Neuroinform.*, 16.
- Chatterjee, S., Thakur, R. S., Yadav, R. N., Gupta, L., and Raghuvanshi, D. K. (2020). Review of noise removal techniques in ECG signals. *IET Signal Processing*, 14(9):569–590.
- Chen, L., Yu, H., Huang, Y., and Jin, H. (2021). ECG Signal-Enabled Automatic Diagnosis Technology of Heart Failure. *J Healthc Eng*, 2021:5802722.
- Chiang, H.-T., Hsieh, Y.-Y., Fu, S.-W., Hung, K.-H., Tsao, Y., and Chien, S.-Y. (2019). Noise Reduction in ECG Signals Using Fully Convolutional Denoising Autoencoders. *IEEE Access*, 7:60806–60813.
- Christov, I. I. (2004). Real time electrocardiogram QRS detection using combined adaptive threshold. *BioMedical Engineering OnLine*, 3(1):28.
- Clifford, G. D., Behar, J., Li, Q., and Rezek, I. (2012). Signal quality indices and data fusion for determining clinical acceptability of electrocardiograms. *Physiol. Meas.*, 33(9):1419–1433.
- Goodfellow, I., Bengio, Y., and Courville, A. (2016). *Deep Learning*. Adaptive Computation and Machine Learning. The MIT Press, Cambridge, Massachusetts.
- Hamilton, P. (2002). Open source ECG analysis. In *Computers in Cardiology*, pages 101–104.
- Huerta, A., Martinez-Rodrigo, A., Rieta, J., Alcaraz, R., and IEEE (2021). ECG Quality Assessment via Deep Learning and Data Augmentation. In *2021 CINC*.
- Kavanagh, J. J. and Menz, H. B. (2008). Accelerometry: A technique for quantifying movement patterns during walking. *Gait & Posture*, 28(1):1–15.
- Kingma, D. P. and Ba, J. (2014). Adam: A Method for Stochastic Optimization.
- Kutz, M. (2010). *Biomedical Engineering and Design Handbook, Volumes I and II (2nd Edition)*. McGraw-Hill Professional Publishing, New York, USA.
- Li, Q., Mark, R. G., and Clifford, G. D. (2007). Robust heart rate estimation from multiple asynchronous noisy sources using signal quality indices and a Kalman filter. *Physiol. Meas.*, 29(1):15–32.
- Li, Q., Rajagopalan, C., and Clifford, G. D. (2014). A machine learning approach to multi-level ECG signal quality classification. *Comp. Methods Prog. Biomed.*, 117(3):435–447.
- Mohaddes, F., da Silva, R. L., Akbulut, F. P., Zhou, Y., Tanneeru, A., Lobaton, E., Lee, B., and Misra, V. (2020). A Pipeline for Adaptive Filtering and Transformation of Noisy Left-Arm ECG to Its Surrogate Chest Signal. *Electronics*, 9(5):866.
- Mohd Apandi, Z. F., Ikeura, R., Hayakawa, S., and Tsutsumi, S. (2020). An Analysis of the Effects of Noisy Electrocardiogram Signal on Heartbeat Detection Performance. *Bioengineering (Basel)*, 7(2):53.
- Munoz-Minjares, J. U., Lopez-Ramirez, M., Vazquez-Olguin, M., Lastre-Dominguez, C., and Shmaliy, Y. S. (2021). Outliers detection for accurate HRV-seizure baseline estimation using modern numerical. *Biomedical Signal Processing and Control*, 67.
- Nonaka, N. and Seita, J. (2022). RandECG: Data Augmentation for Deep Neural Network Based ECG Classification. In Takama, Y., Matsumura, N., Yada, K., Matsushita, M., Katagami, D., Abe, A., Kashima, H., Hiraoka, T., Uchiya, T., and Rzepka, R., editors, *Advances in Art. Intel.*, volume 1423, pages 178–189.
- Nurmaini, S., Darmawahyuni, A., Sakti Mukti, A. N., Rachmatullah, M. N., Firdaus, F., and Tutuko, B. (2020). Deep Learning-Based Stacked Denoising and Autoencoder for ECG Heartbeat Classification. *Electronics*, 9(1):135.
- Pan, Q., Li, X., and Fang, L. (2020). Data Augmentation for Deep Learning-Based ECG Analysis. In *Feature Engineering and Computational Intelligence in ECG Monitoring*, pages 91–111. Springer, Singapore.
- Prieto-Avalos, G., Cruz-Ramos, N. A., Alor-Hernández, G., Sánchez-Cervantes, J. L., Rodríguez-Mazahua, L., and Guarneros-Nolasco, L. R. (2022). Wearable Devices for Physical Monitoring of Heart: A Review. *Biosensors*, 12(5):292.
- Raya, M. and Sison, L. (2002). Adaptive noise cancelling of motion artifact in stress ECG signals using accelerometer. In *Proc. of the 2nd Joint 24th Ann. Conf. and the Ann. Fall Meeting of the Biomedical Eng. Soc. (IEMBS)*, volume 2, pages 1756–1757 vol.2.
- Reljin, N., Lazaro, J., Hossain, M. B., Noh, Y. S., Cho, C. H., and Chon, K. H. (2020). Using the Redundant Convolutional Encoder–Decoder to Denoise QRS Complexes in ECG Signals Recorded with an Armband Wearable Device. *Sensors*, 20(16):4611.
- Rodrigues, J., Belo, D., and Gamboa, H. (2017). Noise detection on ECG based on agglomerative clustering of morphological features. *Computers in Biology and Medicine*, 87:322–334.
- Saraiva, J. (nov-2022a). *Deep Residual Learning for Epileptic Seizure Prediction and Tools to Expedite Biosignal Research*. MSc. Thesis, Department of Computer Science and Engineering, Instituto Superior Técnico, Universidade de Lisboa, Lisbon.

- Saraiva, J. (nov-2022b). *Denoising and Artifact Removal of Ambulatory Electrocardiogram for Patient Continuous-Monitoring*. MSc. Thesis, Department of Bioengineering, Instituto Superior Técnico, Universidade de Lisboa, Lisbon.
- Semmlow, J. L. and Griffel, B. (2014). *Biosignal and Medical Image Processing*. CRC Press, 3rd ed. edition.
- Vandecasteele, K., Cooman, T. D., Chatzichristos, C., Cleeren, E., Swinnen, L., Ortiz, J. M., Huffel, S. V., Dümpelmann, M., Schulze-Bonhage, A., Vos, M. D., Paesschen, W. V., and Hunyadi, B. (2021). The power of ECG in multimodal patient-specific seizure monitoring: Added value to an EEG-based detector using limited channels. *Epilepsia*, 62(10).
- Xia, Y., Zhang, H., Xu, L., Gao, Z., Zhang, H., Liu, H., and Li, S. (2018). An Automatic Cardiac Arrhythmia Classification System With Wearable Electrocardiogram. *IEEE Access*, 6:16529–16538.
- Xiong, P., Wang, H., Liu, M., and Liu, X. (2015). Denoising Autoencoder for Electrocardiogram Signal Enhancement. *Journal of Medical Imaging and Health Informatics*, 5(8):1804–1810.

